


Spontaneous symmetry breaking induced thermospin effect in superconducting tunnel junctionsGaia Germanese^{1,2}, Federico Paolucci², Giampiero Marchegiani³, Alessandro Braggio² and Francesco Giazotto²¹*Dipartimento di Fisica dell'Università di Pisa, Largo Pontecorvo 3, I-56127 Pisa, Italy*²*NEST Istituto Nanoscienze-CNR and Scuola Normale Superiore, I-56127 Pisa, Italy*³*Quantum Research Centre, Technology Innovation Institute, Abu Dhabi, P.O. Box 9639, United Arab Emirates* (Received 4 May 2021; revised 22 October 2021; accepted 26 October 2021; published 8 November 2021)

We discuss the charge and the spin tunneling currents between two Bardeen-Cooper-Schrieffer (BCS) superconductors, where one density of states is spin-split by the proximity of a ferromagnetic insulator. In the presence of a large temperature bias across the junction, we predict the generation of a spin-polarized thermoelectric current. This thermospin effect is the result of a spontaneous particle-hole symmetry breaking in the absence of any polarizing tunnel barrier. The two spin components, which move in opposite directions, generate a spin current larger than the purely polarized case when the thermoactive component dominates over the dissipative one.

DOI: [10.1103/PhysRevB.104.184502](https://doi.org/10.1103/PhysRevB.104.184502)**I. INTRODUCTION**

Spintronics consists of the active manipulation of the spin degree of freedom to develop a wide range of solid-state technologies [1,2]. In this context, hybrid systems involving ferromagnets and superconductors have been exploited for the generation of spin-polarized currents [3–10] with applications as memory elements [11–14] due to a nearly perfect spin-valve effect. At the same time, thermoelectricity in these hybrid devices has been discussed theoretically [15–19] and experimentally [20–24] with intriguing results at the non-local level [25–31] and applications as detectors [32]. Yet, in the presence of temperature gradients, the interplay of the magnetic field with the superconducting order parameter gives rise to exotic nonequilibrium phenomena, such as the generation of pure spin currents (spin-Seebeck effect) [33–38]. Particle-hole (PH) symmetry breaking is a necessary requirement to generate thermoelectricity in the linear regime, i.e., $\delta V, \delta T \rightarrow 0$ [39,40]. In particular, the violation of this symmetry in ferromagnet-superconductor systems was theoretically demonstrated in the presence of magnetic impurities, which strongly enhance the thermoelectric coefficient [41,42]. This limitation can be overcome in the presence of a large temperature bias (nonlinear regime), as recently demonstrated in tunnel junctions between superconductors with different energy gaps [43,44].

Here, we investigate the thermospin effect induced by spontaneous PH symmetry breaking in hybrid ferromagnetic insulator/superconductor systems for a large temperature bias. The effect shares some similarities with the physics reported in Ref. [43], such as the bipolar thermoelectric nature. On the other hand, it is very different in character since the spin-splitting generates a spin current and charge thermoelectricity even for superconductors of identical gaps. In these conditions, counterintuitively, dissipative and thermoactive opposite spin components coexist, resulting in maximal spin

current efficiency and thermoelectric power generation. We consider a thermally biased heterostructure of tunnel junctions [see Fig. 1(a)]. The system is composed by a Bardeen-Cooper-Schrieffer (BCS) superconductor (S) coupled with a ferromagnetic superconductor (S_m) by an insulating barrier (I). The magnetization of S_m is induced by an exchange interaction due to the proximity of a ferromagnetic insulator (FI) when the thickness of S_m (d) is smaller than the coherence length [45,46]. This geometry has been realized in recent experiments [47,48]. In this system, the exchange interaction (h_{exc}) breaks the degeneracy between the spin-up (\uparrow) and spin-down (\downarrow) components of the superconducting density of states (DoS) [49].

We first give an intuitive description of the effect by analyzing the charge current (I_q) and the spin current (I_s) in the presence of a thermal bias, i.e., $T_S > T_{S_m}$, where T_S (T_{S_m}) is the quasiparticle temperature of S (S_m). Figure 1(b) shows I_q (solid curves) as a function of the bias voltage (V) in the absence [black, see also left energy diagram in the box of Fig. 1(a)], and in the presence [aquamarine, see also right energy diagram in the box of Fig. 1(a)] of a sizable h_{exc} . In both cases, I_q is linear in the voltage bias ($I_q \propto V$) for large V (Ohmic response). For low values of V , the trace is highly nonlinear and current peaks appear, corresponding to the matching between the singularities in the superconducting DoS [50]. Note that each of the two antisymmetric peaks in the $I_q(V)$ characteristics for $h_{\text{exc}} = 0$ is doubled for $h_{\text{exc}} \neq 0$ since the spin-degeneracy is broken by the exchange interaction. In the inset, we magnify the low-voltage behavior (dashed-rectangle), and we include the corresponding spin current (dashed lines). Clearly, I_s is exactly zero for $h_{\text{exc}} = 0$, and finite for $h_{\text{exc}} \neq 0$. Moreover, I_q flows against the bias voltage for small values of V when $h_{\text{exc}} \neq 0$, i.e., the junction produces thermoelectric power, while it is always dissipative for $h_{\text{exc}} = 0$. When the active thermospin current is generated, it results in $|I_s| > |I_q|$. This inequality is never realized in a

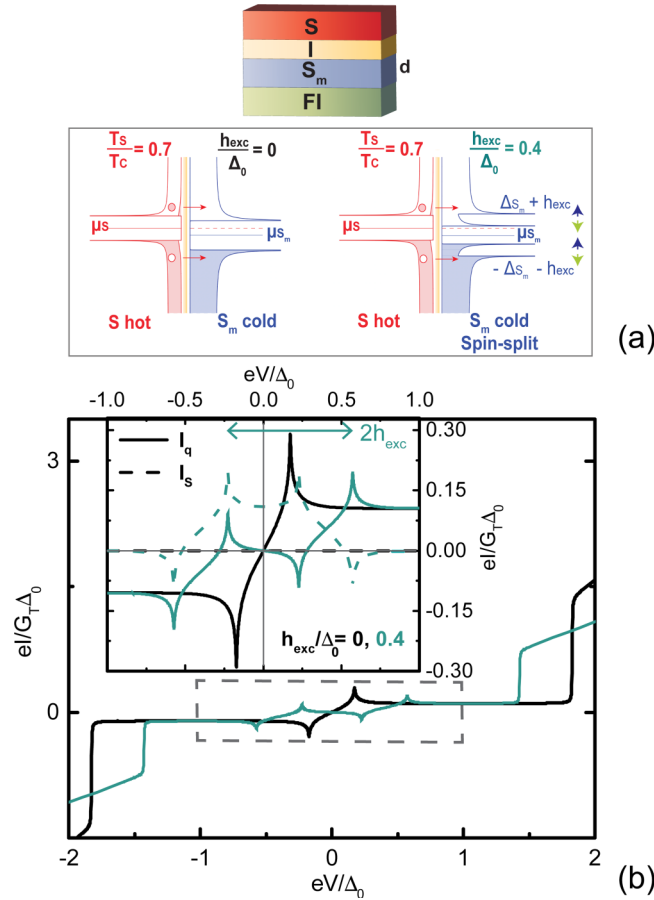


FIG. 1. (a) Top: S - I - S_m junction building blocks. The top hot (bottom cold) superconductor is indicated with S (S_m), and the exchange field is present in S_m only. Bottom: Energy band diagrams of the superconductors are shown in the absence ($h_{\text{exc}} = 0$, left panel) and presence ($h_{\text{exc}} = 0.4\Delta_0$, right panel) of an exchange field (h_{exc}). For $h_{\text{exc}} = 0$, the DoS of S_m exhibits two peaks. For $h_{\text{exc}} = 0.4\Delta_0$, the spin-split DoS (blue \uparrow and green \downarrow for the up and down spin components, respectively) shows four peaks. The difference between the chemical potential of the two leads is $\mu_S - \mu_{S_m} = eV$. The temperature of the S (S_m) superconductor is set at $T_S = 0.7T_c$ ($T_{S_m} = 0.01T_c$). (b) Quasiparticle current-voltage characteristics for $h_{\text{exc}} = 0$ (black) and $h_{\text{exc}} = 0.4\Delta_0$ (aquamarine) display two and four matching peaks, respectively. Inset: Blow-up of the charge (I_q , solid lines) and spin currents (I_s , dashed lines) at low bias voltage.

perfect spin-polarized barrier (i.e., 100% polarization), where $|I_s| = |I_q|$ [1]. Indeed, in our structure, the two finite spin-current components (I_\uparrow and I_\downarrow) flow in opposite directions. Moreover, when the thermoelectric component dominates, a net thermoelectric spin-polarized current occurs.

II. MODEL

We assume S_m to be much thinner than its superconducting coherence length ($d \ll \xi_{0,m}$), to consider a homogeneous exchange interaction in S_m [45]. The normalized DoS of the spin- σ component [with $\sigma = +(\uparrow), -(\downarrow)$] for the α

superconducting electrode (with $\alpha = S, S_m$) is expressed as

$$N_{\alpha\sigma}(E_\alpha) = \left| \text{Re} \left[\frac{E_\alpha + \sigma h_\alpha + i\Gamma}{\sqrt{(E_\alpha + \sigma h_\alpha + i\Gamma)^2 - \Delta_\alpha^2}} \right] \right|, \quad (1)$$

where h_α is the exchange field, $E_\alpha = E - \mu_\alpha$ is the quasiparticle energy measured with respect to the chemical potential μ_α [51], Δ_α is the self-consistent superconducting energy gap for the α -lead [52], and Γ is the phenomenological Dynes parameter [53,54]. The sum of the two spin contributions gives the total DoS of a spin-split superconductor $N_\alpha(E) = \sum_{\sigma=\pm} N_{\alpha\sigma}(E)/2$. We will adopt the usual approximations found to be valid in many experiments [55]. For $\alpha = S$, we assume $h_S = 0$. Note that, even in the presence of an exchange field, the DoS is PH symmetric, i.e., $N_\alpha(E_\alpha) = N_\alpha(-E_\alpha)$ [56], and the spin component satisfies $N_{\alpha\sigma}(E_\alpha) = N_{\alpha\bar{\sigma}}(-E_\alpha)$, with $\bar{\sigma} = -\sigma$.

The quasiparticle current of the spin- σ component reads

$$I_\sigma = \frac{G_T}{2e} \int_{-\infty}^{\infty} dE N_{S\sigma}(E - eV) N_{S_m\sigma}(E) F_{SS_m}(E), \quad (2)$$

where e is the electron charge, G_T is the normal-state conductance of the tunnel junction [57], and $F_{SS_m}(E) = f_S(E - eV) - f_{S_m}(E)$ is the difference between the Fermi-Dirac quasiparticle distributions of two electrodes $f_\alpha(E, T_\alpha) = [1 + \exp(E/k_B T_\alpha)]^{-1}$ with $\alpha = S, S_m$. We assume to work in the quasi-equilibrium regime, where each electrode is separately at the thermal equilibrium and the electronic temperature can differ from the phononic one, as experimentally demonstrated [58–61]. The charge current and the spin current are defined as $I_q = I_\uparrow + I_\downarrow$ and $I_s = I_\uparrow - I_\downarrow$, respectively. By exploiting the PH symmetry, we note that the charge current is odd (even) in V (h_{exc}) with $I_q(V, h_{\text{exc}}) = -I_q(-V, h_{\text{exc}}) = I_q(V, -h_{\text{exc}})$, while the spin current is an even (odd) function in V (h_{exc}) with $I_s(V, h_{\text{exc}}) = I_s(-V, h_{\text{exc}}) = -I_s(V, -h_{\text{exc}})$, as shown in Fig. 1(b) [62].

We assume the two superconductors (S and S_m) to have the same zero-temperature energy gap ($\Delta_{S,0} = \Delta_{S_m,0} = \Delta_0$) and, hence, the same critical temperature T_c . Therefore, no thermoelectric effect occurs for $h_{\text{exc}} = 0$ [43,44].

III. CHARGE THERMOELECTRIC EFFECT

Here, we investigate thermoelectric effects in the S - I - S_m junction as a function of the thermal bias and exchange field. Typical current-voltage characteristics for different values of h_{exc} at $T_S = 0.7T_c$ and $T_{S_m} = 0.01T_c$ are shown in Fig. 2(a). For $h_{\text{exc}} = 0$ (black solid line), the system is dissipative [$I_q(V)V > 0$], and the current displays subgap peaks at $V = \pm V_p = \pm |\Delta(T_S) - \Delta(T_{S_m})|/|e|$. It is enough of a weak exchange field ($h_{\text{exc}} = 0.1\Delta_0$, magenta solid line) to observe the splitting of the peaks at $V = \pm V_p^\mp = \pm |\Delta(T_S) - \Delta(T_{S_m}) \pm h_{\text{exc}}|/|e|$. For larger values of the exchange field ($h_{\text{exc}} \gtrsim 0.2\Delta_0$), a thermoelectric power is generated [$I_q(V)V < 0$]. Thermodynamic analysis [43] shows that in a thermally biased nonequilibrium system the generation of thermopower in the junction is possible, which corresponds to an absolute negative conductance (ANC) [62]. The exchange field spontaneously generates a thermospin effect (discussed in more details below). The spin-splitting in S_m is fundamental to activate this effect when $\Delta_{S,0} = \Delta_{S_m,0}$. Indeed, the spin-splitting

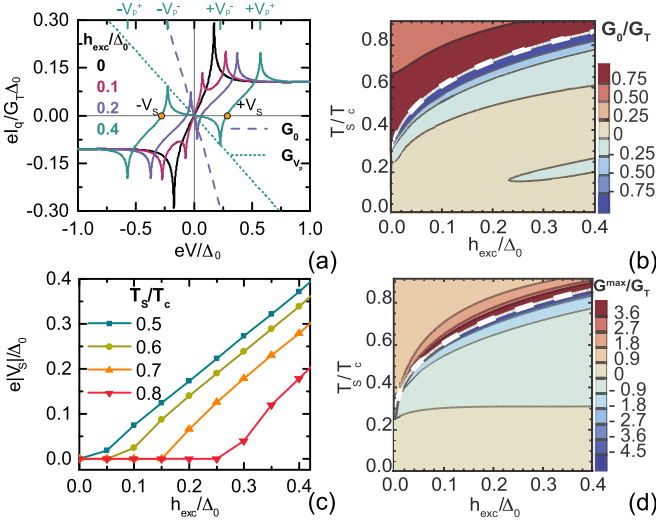


FIG. 2. (a) Quasiparticle current-voltage $I_q(V)$ characteristics are shown for different values of h_{exc}/Δ_0 . In the linear regime, the IV curves can be approximated by the linear $I_q = G_0V$ of Eq. (3) (dashed violet line), while, in the nonlinear regime in bias, the G^{max} evaluated at the thermoelectric peaks (dotted aquamarine line). The Seebeck voltages ($\pm V_S$) (orange circles) and the matching peak values ($\pm V_p^\pm$) are reported for $h_{exc} = 0.4\Delta_0$. (b) In the linear regime, the zero-bias conductance (G_0) as a function of h_{exc} and T_S is shown, distinguishing thermoactive areas (blue tones) from dissipative ones (red tones). (c) Absolute value of the Seebeck voltage as a function of h_{exc} is shown for different values of the thermal bias (T_S). (d) Maximum conductance evaluated at the matching peak V_p^- is displayed as a function of T_S and h_{exc} in the nonlinear regime. The blue tones are linked to the negative conductance (thermoelectricity), while the red area is referred to the positive one (dissipation).

in the bottom electrode DoS effectively reduces the gap, and, at the same time, localizes purely spin-polarized states between $\Delta_{S_m} - h_{exc}$ and $\Delta_{S_m} + h_{exc}$. These combined mechanisms determine a spontaneous spin-Seebeck effect, leading to thermoelectricity and ANC, that is, $G(V) = I_q(V)/V < 0$. For $V \rightarrow 0$, the conductance can be approximated by

$$\frac{G_0}{G_T} \simeq -\Delta_0^2 \sum_{\sigma} \int_0^{\infty} dE \frac{N_S(E) f_{S_m}(E, T_{S_m})}{[(E + i\Gamma + \sigma h_{exc})^2 - \Delta_0^2]^{3/2}}. \quad (3)$$

See, for instance, the dashed violet line ($I_q = G_0V$) for $h_{exc} = 0.2\Delta_0$ in Fig. 2(a). Equation (3) holds only for $\Delta(T_S) > \Delta(T_{S_m}) - h_{exc}$, that is, when thermoelectricity appears. Figure 2(b) displays G_0 computed through numerical differentiation of I_q as a function of T_S/T_c and h_{exc}/Δ_0 . We can distinguish thermoelectric ($G_0 < 0$, blue) and dissipative ($G_0 > 0$, red) areas. For a fixed h_{exc} , thermoelectricity is present only in a limited range of T_S . In particular, the maximum value of T_S providing a thermoelectric effect is due to the condition $\Delta(T_S) > \Delta(T_{S_m}) - h_{exc}$ (dashed white line). This constrain corresponds to the requirement to have the hot electrode with the largest “effective” gap [43,44].

The thermoelectric power is typically maximum at the internal peak voltages $V = \pm V_p^\pm = \pm |\Delta(T_S) - [\Delta(T_{S_m}) - h_{exc}]|/|e|$. Being $\Delta(T_S) < \Delta(T_{S_m})$, we note that $|V_p^-|$ can be increased by raising h_{exc} . As a consequence, the generated

maximum thermopower $-I_q(V_p^-)V_p^-$ is expected to increase accordingly. Note that h_{exc} cannot be freely increased due to the Chandrasekhar-Clogston limit ($h_{exc} \leq \Delta_0/\sqrt{2}$) [63–65].

A typical thermoelectric figure of merit is the Seebeck voltage (V_S), which represents the bias that stops the thermocurrent $I_q(V_S) = 0$ [see the orange circles in Fig. 2(a)]. $|V_S|$ grows monotonically with h_{exc} , as shown in Fig. 2(c) for different values of T_S , and its maximum is limited again by the Chandrasekhar-Clogston limit [62]. Moreover, $|V_S|$ increases by lowering T_S , which corresponds to a decrease of the thermal gradient. This odd behavior shows that thermoelectricity is purely nonlinear [43], and notably different from thermoelectricity in the linear regime [34]. Another significant figure of merit is the ratio between the maximum thermoelectric current and the corresponding voltage, i.e., $G^{max} \sim I_q^\pm(V_p^\pm)/V_p^\pm$ [see aquamarine dotted line for $h_{exc} = 0.4\Delta_0$ in Fig. 2(a)]. This quantity plays a crucial role when the thermoelectric element is connected to a load. More precisely, $-G^{max}$ represents the maximal I_q conductance of the load supported by the thermoelectric junction, such as no net thermopower can be generated if the load conductance is bigger than $-G^{max}$ [44,62]. Figure 2(d) shows G^{max} as a function of h_{exc} and T_S . We can identify again thermoelectric ($G^{max} < 0$, blue) and dissipative ($G^{max} > 0$, red) regimes. We find that the temperature range where the junction is thermoactive widens by increasing h_{exc} . Indeed, for a given h_{exc} , the maximum value of T_S is still limited by the above-mentioned relation for G_0 [dashed white line of Figs. 2(b) to 2(d)]. For low temperatures, thermoelectricity disappears arising from the nonlinear nature of the effect in temperature [66]. Some other differences between Figs. 2(b) and 2(d) are discussed in more detail in Ref. [62].

IV. SPIN THERMOELECTRIC EFFECT

Here, we investigate the thermospin current, which represents another peculiar consequence of spin symmetry breaking in the setup considered.

Figure 3(a) shows typical charge current (I_q , aquamarine line) and spin current (I_s , orange dashed line) as a function of V in the presence of thermoelectricity. In addition, we consider the two spin components of I_q , i.e., I_\uparrow (spin up, blue line) and I_\downarrow (spin down, light green line). At $V = 0$, $I_q(V = 0) = 0$, due to PH symmetry. Still, the two spin components are finite, and exactly opposite since $h_{exc} \neq 0$. Therefore, one of the spin components is thermoactive [in Fig. 3(a) $I_\uparrow(V)V < 0$ for $V < 0$, $I_\downarrow(V)V < 0$ for $V > 0$], while the other one is dissipative. Thus, the system produces spin-polarized thermoelectricity when the thermoactive component is larger than the dissipative one. Interestingly, the Seebeck voltage represents the bias where the thermoactive and dissipative components compensate, i.e., $I_\uparrow(+V_S) = -I_\downarrow(+V_S)$ such as $I_q(\pm V_S) = 0$, thus obtaining a purely spin current. Moreover, the maximum spin current is located at the internal matching peaks ($\pm V_p^\pm$).

Hence, it is convenient to introduce a new figure of merit, which compares the spin current generated by the system with respect to all the carriers moving across the junction. We define the spin current generation efficiency as $SGE = I_s/(|I_\uparrow| + |I_\downarrow|)$. Note that when the two spin components flow in opposite directions $|I_s| > |I_q|$ and the system is globally thermoactive [$I_q(V)V < 0$], necessarily $SGE = 1$. Figure 3(b)

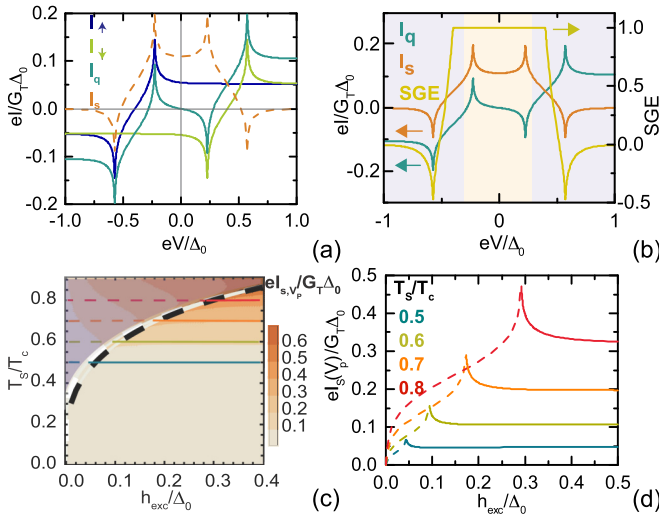


FIG. 3. (a) The charge current (I_q) is separated into up (I_\uparrow) and down (I_\downarrow) spin components for $h_{\text{exc}} = 0.4\Delta_0$. Only one spin component (I_\downarrow for $V > 0$, I_\uparrow for $V < 0$) generates a thermoactive peak. The spin current (I_s) is reported in the dashed orange line. (b) The IV characteristics of the charge current (I_q) and spin current (I_s) and the curve of the spin current generation efficiency (SGE) are displayed for $h_{\text{exc}} = 0.4\Delta_0$. The yellow area between the Seebeck voltages ($\pm V_s$) highlights the thermoactive spin current generation, while in the violet area the system is dissipative behaving as a spin filter. (c) The spin current evaluated at $+V_p^-$ is reported as a function of T_S and h_{exc} . Fixing T_S (colored lines), the maximal value of I_s is reached for the optimal value of h_{exc} such as $\Delta_S = \Delta_{S_m} - h_{\text{exc}}$ (dashed white line). With a black dashed line, we show the approximation of h_{exc}^t . The violet transparent zone highlights the dissipative behavior of the system. (d) The maximum spin current, evaluated at the matching peak voltage ($+V_p^-$), corresponding to the colored cuts of the previous panel (c) (dashed lines for the dissipative regime and solid lines for the thermoelectric regime), is shown as a function of h_{exc} for different values of T_S .

displays SGE as a function of V , for the curves in Fig. 3(a). For $|V| > V_s$, where the junction is dissipative (violet area), we can distinguish two behaviors. The first is characterized by $\text{SGE} = 1$ with a thermoactive spin component but lower than the dissipative one, i.e., no charge thermopower is generated. In the second case, $\text{SGE} < 1$. Here, both spin components are dissipative and the total charge current flows in the same direction of the bias. The current is still spin-polarized, but $|I_s| \leq |I_q|$ similarly to a spin-polarizer [34–36]. For large $|V|$, the total current is almost independent of the spin-splitting, and the two components give the same contribution, leading to $I_s \rightarrow 0$.

In Fig. 3(c), we analyze the maximal spin current evaluated at the peak $I_s(\pm V_p^-)$ as a function of h_{exc} and T_S . At fixed h_{exc} ,

I_s increases with the thermal bias $\delta T = T_S - T_{S_m} \sim T_S$. By contrast, for a given thermal gradient (δT , colored cuts), the spin current is nonmonotonic in h_{exc} , reaching the maximum value for $h_{\text{exc}} = \Delta(T_{S_m}) - \Delta(T_S)$. This condition coincides with the threshold value of the exchange field [$h_{\text{exc}}^t(T_S)$] to generate thermoelectricity, which can be estimated as $h_{\text{exc}}^t = \Delta(1 - \tanh[1.74\sqrt{(T_c/T_S) - 1}])$ [62]. Its approximate value is displayed in Fig. 3(c) with a black dashed line. In particular, for a fixed T_S , spin-thermoelectricity occurs only for $h_{\text{exc}} \geq h_{\text{exc}}^t$ (solid part of the colored cuts), otherwise, it is dissipative (dashed part). Finally, Fig. 3(d) shows $I_s(\pm V_p^-)$ as a function of h_{exc} for selected values of T_S . In particular, $I_s(V_p^-)$ grows with T_S , reaching its maximum at h_{exc}^t . We observe that the maximum value of the thermocurrent is of the order of $I_s^{\text{max}} \sim 0.5G_T\Delta_0/e$. Assuming the aluminium gap of $\Delta_0 = 200\mu\text{eV}$ and tunneling conductance of $G_T = 0.1\text{ mS}$, we expect spin currents of the order of 10 nA. Spin currents cannot be easily detected without further elaborating on the design. Possible methods are measuring spin accumulation phenomena or employing spin-filtering.

V. CONCLUSION

In summary, we discussed the nonlinear thermospin effect, generated in a thermally biased S - I - S_m Josephson junction in the presence of an exchange interaction. This effect is generated by the spontaneous particle-hole symmetry breaking activated by spin-splitting in S_m . By exploiting the two spin current components that the system naturally drives in opposite direction, we observe the coexistence of one spin thermoactive with one dissipative component. Notably, the spin thermoelectricity is relevant when the thermoactivated component dominates, thus obtaining $|I_s| > |I_q|$. Our results suggest interesting applications in thermoelectricity [40], low-dissipative and thermoactive spintronics [1,35], and radiation detection [67].

ACKNOWLEDGMENTS

We acknowledge the European Research Council under Grant Agreement No. 899315-TERASEC, and the EUs Horizon 2020 research and innovation program under Grant Agreements No. 800923 (SUPERTED) and No. 964398 (SUPERGATE) for partial financial support. The Royal Society through the International Exchanges between the UK and Italy (Grant No. IEC R2 192166), and the SNS-WIS joint laboratory QUANTRA funded by the Italian Ministry of Foreign Affairs and International Cooperation.

- [1] I. Žutić, J. Fabian, and S. Das Sarma, *Rev. Mod. Phys.* **76**, 323 (2004).
- [2] J. Linder and J. W. A. Robinson, *Nat. Phys.* **11**, 307 (2015).
- [3] P. M. Tedrow and R. Meservey, *Phys. Rev. Lett.* **27**, 919 (1971).

- [4] R. Meservey, P. M. Tedrow, and R. C. Bruno, *Phys. Rev. B* **11**, 4224 (1975).
- [5] S. Takahashi, H. Imamura, and S. Maekawa, *Phys. Rev. Lett.* **82**, 3911 (1999).

- [6] F. J. Jedema, B. J. van Wees, B. H. Hoving, A. T. Filip, and T. M. Klapwijk, *Phys. Rev. B* **60**, 16549 (1999).
- [7] S. Takahashi, T. Yamashita, T. Koyama, S. Maekawa, and H. Imamura, *J. Appl. Phys.* **89**, 7505 (2001).
- [8] T. Yamashita, S. Takahashi, H. Imamura, and S. Maekawa, *Phys. Rev. B* **65**, 172509 (2002).
- [9] S. Maekawa, S. Takahashi, and H. Imamura, *J. Phys. D* **35**, 2452 (2002).
- [10] F. Giazotto and F. Taddei, *Phys. Rev. B* **77**, 132501 (2008).
- [11] X. Hao, J. S. Moodera, and R. Meservey, *Phys. Rev. B* **42**, 8235 (1990).
- [12] F. Giazotto, *Appl. Phys. Lett.* **95**, 042503 (2009).
- [13] F. S. Bergeret, A. Verso, and A. F. Volkov, *Phys. Rev. B* **86**, 214516 (2012).
- [14] G. De Simoni, E. Strambini, J. S. Moodera, F. S. Bergeret, and F. Giazotto, *Nano Lett.* **18**, 6369 (2018).
- [15] P. Virtanen and T. T. Heikkilä, *J. Low Temp. Phys.* **136**, 401 (2004).
- [16] M. Titov, *Phys. Rev. B* **78**, 224521 (2008).
- [17] P. Jacquod and R. S. Whitney, *Europhys. Lett.* **91**, 67009 (2010).
- [18] M. S. Kalenkov and A. D. Zaikin, *Phys. Rev. B* **95**, 024518 (2017).
- [19] J. Heidrich and D. Beckmann, *Phys. Rev. B* **100**, 134501 (2019).
- [20] J. Eom, C.-J. Chien, and V. Chandrasekhar, *Phys. Rev. Lett.* **81**, 437 (1998).
- [21] A. Parsons, I. A. Sosnin, and V. T. Petrashov, *Phys. Rev. B* **67**, 140502(R) (2003).
- [22] Z. Jiang and V. Chandrasekhar, *Phys. Rev. B* **72**, 020502(R) (2005).
- [23] F. Giazotto, P. Solinas, A. Braggio, and F. S. Bergeret, *Phys. Rev. Appl.* **4**, 044016 (2015).
- [24] Z. B. Tan, A. Laitinen, N. S. Kirsanov, P. J. Hakonen, A. Galda, V. M. Vinokur, M. Haque, A. Savin, D. S. Golubev, G. B. Lesovik, and P. J. Hakonen, *Nat. Commun.* **12**, 138 (2021).
- [25] P. Virtanen and T. T. Heikkilä, *Phys. Rev. Lett.* **92**, 177004 (2004).
- [26] P. E. Dolgirev, M. S. Kalenkov, and A. D. Zaikin, *Phys. Rev. B* **97**, 054521 (2018).
- [27] R. Hussein, M. Governale, S. Kohler, W. Belzig, F. Giazotto, and A. Braggio, *Phys. Rev. B* **99**, 075429 (2019).
- [28] N. S. Kirsanov, Z. B. Tan, D. S. Golubev, P. J. Hakonen, and G. B. Lesovik, *Phys. Rev. B* **99**, 115127 (2019).
- [29] G. Blasi, F. Taddei, L. Arrachea, M. Carrega, and A. Braggio, *Phys. Rev. Lett.* **124**, 227701 (2020).
- [30] G. Blasi, F. Taddei, L. Arrachea, M. Carrega, and A. Braggio, *Phys. Rev. B* **102**, 241302(R) (2020).
- [31] M. S. Kalenkov, P. E. Dolgirev, and A. D. Zaikin, *Phys. Rev. B* **101**, 180505(R) (2020).
- [32] T. T. Heikkilä, R. Ojajarvi, I. J. Maasilta, E. Strambini, F. Giazotto, and F. S. Bergeret, *Phys. Rev. Appl.* **10**, 034053 (2018).
- [33] P. Machon, M. Eschrig, and W. Belzig, *Phys. Rev. Lett.* **110**, 047002 (2013).
- [34] A. Ozaeta, P. Virtanen, F. S. Bergeret, and T. T. Heikkilä, *Phys. Rev. Lett.* **112**, 057001 (2014).
- [35] J. Linder and M. E. Bathen, *Phys. Rev. B* **93**, 224509 (2016).
- [36] F. S. Bergeret, M. Silaev, P. Virtanen, and T. T. Heikkilä, *Rev. Mod. Phys.* **90**, 041001 (2018).
- [37] S. Kolenda, C. Sürgers, G. Fischer, and D. Beckmann, *Phys. Rev. B* **95**, 224505 (2017).
- [38] D. S. Shapiro, D. E. Feldman, A. D. Mirlin, and A. Shnirman, *Phys. Rev. B* **95**, 195425 (2017).
- [39] D. Sánchez and R. López, *C. R. Phys.* **17**, 1060 (2016).
- [40] G. Benenti, G. Casati, K. Saito, and R. S. Whitney, *Phys. Rep.* **694**, 1 (2017).
- [41] Z. A. D. Kalenkov, A. D. Zaikin, and L. S. Kuzmin, *Phys. Rev. Lett.* **109**, 147004 (2012).
- [42] M. S. Kalenkov and A. D. Zaikin, *Phys. Rev. B* **90**, 134502 (2014).
- [43] G. Marchegiani, A. Braggio, and F. Giazotto, *Phys. Rev. Lett.* **124**, 106801 (2020).
- [44] G. Marchegiani, A. Braggio, and F. Giazotto, *Phys. Rev. B* **101**, 214509 (2020).
- [45] T. Tokuyasu, J. A. Sauls, and D. Rainer, *Phys. Rev. B* **38**, 8823 (1988).
- [46] X. Hao, J. S. Moodera, and R. Meservey, *Phys. Rev. Lett.* **67**, 1342 (1991).
- [47] E. Strambini, V. N. Golovach, G. De Simoni, J. S. Moodera, F. S. Bergeret, and F. Giazotto, *Phys. Rev. Materials* **1**, 054402 (2017).
- [48] A. Hijano, S. Ilić, M. Rouco, C. González-Orellana, M. Ilyn, C. Rogero, P. Virtanen, T. T. Heikkilä, S. Khorshidian, M. Spies, N. Ligato, F. Giazotto, E. Strambini, and F. S. Bergeret, *Phys. Rev. Research* **3**, 023131 (2021).
- [49] We assume the Josephson coupling can be suppressed via Fraunhofer interference, or SQUID interferometry, by applying an in-plane or out-of-plane magnetic field, respectively [68,69].
- [50] S. Shapiro, P. H. Smith, J. Nicol, J. L. Miles, and P. F. Strong, *IBM J. Res. Dev.* **6**, 34 (1962).
- [51] For simplicity, we assume that the chemical potential for the two spin-species is equal $\mu_{\uparrow} = \mu_{\downarrow}$ (no spin accumulation). This approximation holds when the spin-relaxation rate in each electrode is larger than the spin-injection rate. The latter scales with spin current of the junction as $I_s \propto G_T$, i.e., for sufficiently opaque tunneling barrier.
- [52] The self-consistency relation is [23,70]:
- $$\log\left(\frac{\Delta_0}{\Delta_\alpha}\right) = \int_0^{\hbar\omega_D} dE \frac{f_+(E) - f_-(E)}{\sqrt{E^2 + \Delta_\alpha^2}}, \quad (4)$$
- where Δ_0 is the zero-temperature pairing potential in absence of the exchange field, ω_D is the Debye frequency and $f_{\pm}(E) = (1 + \exp[(\sqrt{E^2 + \Delta^2} \mp h_{\text{exc}})/k_B T_R])^{-1}$ with k_B Boltzmann constant.
- [53] R. C. Dynes, J. P. Garno, G. B. Hertel, and T. P. Orlando, *Phys. Rev. Lett.* **53**, 2437 (1984).
- [54] The value of the parameter used for the calculation is $\Gamma = 10^{-3}\Delta_0$, consistent with the state-of-the-art nanofabrication results [48]. A more detailed study of the dependence with Γ can be also found in [62].
- [55] For simplicity, we neglect the spin-flip and spin-orbit effects, which are not universal and material and geometry dependent [14,37,47,48].
- [56] M. Tinkham, *Introduction to Superconductivity* (Dover, Mineola, NY, 2004).
- [57] $G_T = G_{\uparrow} + G_{\downarrow}$ and we assume the two spin to have equally contribute $G_{\uparrow} = G_{\downarrow}$.
- [58] F. Giazotto, T. T. Heikkilä, A. Luukanen, A. M. Savin, and J. P. Pekola, *Rev. Mod. Phys.* **78**, 217 (2006).

- [59] J. T. Muhonen, M. Meschke, and J. P. Pekola, *Rep. Prog. Phys.* **75**, 046501 (2012).
- [60] F. Giazotto and M. Martínez-Pérez, *Nature* **492**, 401 (2012).
- [61] A. Fornieri and F. Giazotto, *Nat. Nanotechnol.* **12**, 944 (2017).
- [62] See Supplemental Material at <http://link.aps.org/supplemental/10.1103/PhysRevB.104.184502> for a more detailed discussion, which includes [71].
- [63] A. M. Clogston, *Phys. Rev. Lett.* **9**, 266 (1962).
- [64] B. S. Chandrasekhar, *Appl. Phys. Lett.* **1**, 7 (1962).
- [65] K. Maki, *Prog. Theor. Phys.* **31**, 731 (1964).
- [66] The lower limit in temperature is nonuniversal, being related to the chosen Γ parameter.
- [67] Z. Geng, A. P. Helenius, T. T. Heikkilä, and I. J. Maasilta, *J. Low Temp. Phys.* **199**, 585 (2020).
- [68] G. Marchegiani, A. Braggio, and F. Giazotto, *Phys. Rev. Research* **2**, 043091 (2020).
- [69] A. Barone, *Principles and Applications of Superconducting Quantum Interference Devices* (World Scientific, Singapore, 1992).
- [70] G. Sarma, *J. Phys. Chem. Solids* **24**, 1029 (1963).
- [71] J. P. Pekola, V. F. Maisi, S. Kafanov, N. Chekurov, A. Kemppinen, Yu. A. Pashkin, O.-P. Saira, M. Möttönen, and J. S. Tsai, *Phys. Rev. Lett.* **105**, 026803 (2010).